ELSEVIER

0308-0161(94)00032-8

Int. J. Pres. Ves. & Piping **64** (1995) 1–10

0308-0161/95/$09.50

Stability analysis of a parabolic pipe-reducer under uniform external pressure

M. Ashiqur Rahman, Md. Raisuddin Khan & Md. Wahhaj Uddin

Department of Mechanical Engineering, Bangladesh University of Engineering and Technology, Dhaka-1000, Bangladesh

(Received 24 April 1994; accepted 6 May 1994)

Truncated parabolic shells can be used to join pipes of unequal diameters instead of the traditional conical reducers; such doubly-curved shell elements are superior to conical shells in withstanding high pressure through the membrane forces. The present investigation analyses the stability of the truncated parabolic shell elements using nonlinear equilibrium equations as the governing equations for the stability of the parabolic reducers. Uddin's computer program with necessary modifications has been used for the present analysis. In this analysis the governing nonlinear equations of shells derived by Reissner are solved by the multisegment integration technique developed by Kalnins and Lestingi. The results show that the critical pressure increases with increase of the diameter ratio. Parabolic reducers are found to be more stable than conical reducers under uniform external pressure.

NOMENCLATURE

a	Distance between the vertex and the focus of the parabola
C, D	Extensional rigidity Eh, bending rigidity $Eh^3/[12(1-\nu^2)]$
E, ν	Young's modulus, Poisson's ratio
h	Shell thickness
H, V	Horizontal and vertical stress resultants
$\bar{H}, \bar{V}$	H/PR, V/PR
k_θ, k_ξ	Curvature changes
$\bar{k}_\theta, \bar{k}_\xi$	$k_\theta\xi_e$, $k_\xi\xi_e$
M_θ, M_ξ	Circumferential and meridional couple resultants
$\bar{M}_\theta, \bar{M}_\xi$	M_θ/PRh, M_ξ/PRh
N_ξ, N_θ	Meridional and circumferential stress resultants
$\bar{N}_\xi, \bar{N}_\theta$	N_ξ/PR, N_θ/PR
$P, \bar{P}, \bar{R}$	external pressure, P/E, ξ_e/R
R_1, R	Smaller and larger radii of the reducer
$r_o, \bar{r}_o$	Radial distance of points on undeformed middle surface from axis of symmetry, r_o/ξ_e
u, w	Radial and axial displacements
$\bar{u}, \bar{w}$	uEh/PR^2, wEh/PR^2
α, β, r	Shell parameter, $\phi_o - \phi$, $r_o + u$
$\epsilon_\xi, \epsilon_\theta$	Middle surface strains
$\bar{\epsilon}_\xi, \bar{\epsilon}_\theta$	$\epsilon_\xi Eh\xi_e/PR^2$, $\epsilon_\theta Eh\xi_e/PR^2$
ϕ_o, ϕ	Angle between axis of symmetry and normal to undeformed and deformed middle surface
ξ_e	Meridional length between centre of the smaller end and the larger end junction
$\xi, \bar{\xi}$	Distance measured along meridian, ξ/ξ_e
σ_c, σ_a	Circumferential and meridional stresses
σ_{ci}, σ_{co}, σ_{ai}, σ_{ao}	Circumferential and meridional stresses at the inner and outer fibres respectively.

1 INTRODUCTION

Reducers used for connecting pipes of unequal diameters are prone to failure by instability when these shell elements are subjected to external pressure or internal suction in practical applications. It was shown by Ali[1] that conical

reducers become more prone to instability as the apex angle of the cone is gradually increased keeping other parameters constant. This is due to the fact that the cone loses its membrane stiffness as the apex angle is gradually increased. On the other hand, a doubly curved parabolic shell has sufficient membrane stiffness and hence is likely to be more stable than the conical reducers. The present analysis primarily deals with the instability of the parabolic reducers of different diameter ratio and thickness ratio.

It should be mentioned here that the stability analysis has been justified for thinner shells with larger diameters. The present analysis is thus for thin reducers with large diameters.

So far most of the theoretical investigations of buckling of shells under pressure, a few examples of which are included in references 8–16, are limited to 'shallow' shells. Even these limited studies have incorporated in them approximations of various kinds, for example approximation in the representation of the geometry of the undeformed shell;[13,16] in the derivation of the governing equations;[12,16] in devising methods of solutions of the governing equations[10,11,13] including the attempt of forcing the shell to deform in a predetermined mode;[8,9,14] and in the final stage in applying some numerical techniques for obtaining solutions of the equations, algebraic or differential, into which the original governing equations are broken down.[10,15,16] The main reason for keeping the studies of stability limited to shallow shells is that the large deflection equations of axisymmetric shells could be solved only when the simplifications pertaining to the shallowness of the shells were made, as pointed out by Uddin.[4,5] The simplified nonlinear differential equations were then solved by different numerical and analytical methods present in the literature.[8–16]

Recent efforts include the development of a number of general-purpose computer programs such as BOSOR5,[17] BOSOR4,[18] ANSR,[19] STAGSC,[20] for shells of revolution based either on finite element or finite difference methods of analyses. Both BOSOR4 and BOSOR5 determine the critical load from an eigenvalue formulation of the problem in which the results of the prebuckled nonlinear analysis of shells, based on the minimization of potential energy, are used. However, as pointed out by Thompson,[7] eigenvalue analysis may lead to an unreliable prediction if the prebuckled state is not accurately determined or not fully taken into account in the eigenvalue formulation. For example, Uddin[5] pointed out that the prediction of BOSOR5 for the critical pressures of shells of revolution are found to be consistently lower than that observed experimentally,[21–25] quite contrary to the general conclusion that the theoretical critical loads of perfect shells are much higher than the test results owing to the initial imperfections in the test specimens. Thus the eigenvalue predictions for critical loads of these two computer programs [BOSOR4 and BOSOR5] are really for shells much weaker than the one considered in the mathematical model. For these reasons the theorems of Thompson and Hunt[7] have been used for the present analysis to anticipate the critical loads for the parabolic reducers; these theorems state that the buckling characteristics of any structure, whatever the type of buckling, may be better comprehended if the equilibrium path of the deformed structure under load is determined for both the prebuckling and postbuckling zones. Thompson's two theorems on buckling[7] point out that the first instability in the equilibrium equations (based on large deformations) on the primary equilibrium configuration path would correspond to the critical load of the structure, irrespective of its type of buckling.

In the present analysis, the governing nonlinear equations of axisymmetric deformations of shells ensuring the unique state of the lowest potential energy are solved for increasing steps of loads. At each load step the appearance of the second solution is searched because this appearance of a second solution according to the 'bifurcation' technique of stability analysis always corresponds to the critical load. However it is found that the numerical solution fails to converge as the critical load is approached and the shell structure deforms enormously.

The multisegment integration technique developed by Kalnins and Lestingi is used here to solve the nonlinear shell equations. This multisegment integration technique is a very powerful tool for handling nonlinear shell equations where either finite element or finite difference technique fails due to nonconvergence of the solution of a large number of equations. This method can be used for shell meridian of any length with discontinuity in slope or thickness where methods like direct integration fail.

2 ANALYSIS

Nonlinear governing equations for axisymmetric deformations of shells, as derived by Reissner[3] and modified by Uddin,[4] are solved by using the method of multisegment integration developed by Kalnins and Lesting[2] with the help of the computer code developed by Uddin.[6] The critical pressure for a particular shell is interpreted from the fact that any further increase in pressure, no matter how small, will cause enormous shell deformation indicating that the state of lowest energy for any increase in pressure is far from that at the critical pressure.

According to Thompson and Hunt[7] the buckling characteristics of any structure, irrespective of the type of buckling, may be best comprehended if the equilibrium path of the deformed structure under load is determined for both the prebuckling and postbuckling zones. Thompson's[7] two theorems on buckling point out that the first instability of the equilibrium equations on the primary equilibrium configuration path would correspond to the critical load of the structure, irrespective of its type of buckling.

Under external loading the shell structures undergo axisymmetric deformations. The mathematical formulation of this problem is a nonlinear one. The symmetric deformation at any load step is first known by numerical solution of six nonlinear first-order ordinary differential equations. These solutions correspond to the equilibrium configurations.

To determine the critical pressure the equilibrium configuration path is traced against increasing load. Here the external loading is increased by small increments and the appearance of a second mode of deformation is looked for. This appearance of a second solution always corresponds to the critical loading; as soon as the bifurcation point is reached the numerical solution no longer converges because the shell structure deforms enormously. The minimum pressure loading for which the solutions fail to converge corresponds to the critical loading.

It should be mentioned here that the term 'bifurcation point' is used to refer to the point of initiation of a secondary mode of deformation, whether it be the limit point or the branching point. This critical pressure is calculated here for various parabolic reducers, varying the diameter ratio and the thickness ratio. The nonlinear governing equations used in the present analysis are presented below. The symbols in the equations are defined in Figs 1, 2 and 3.

$$\bar{\epsilon}_\theta = \frac{\bar{u}}{\bar{r}_o} \tag{1a}$$

$$\phi = \phi_o - \beta \tag{1b}$$

$$\bar{k}_\theta = (\sin\phi_o - \sin\phi)/\bar{r}_o \tag{1c}$$

$$\bar{N}_\xi = \bar{H}\cos\phi + \bar{V}\sin\phi \tag{1d}$$

$$\bar{\epsilon}_\xi = \bar{C}\bar{N}_\xi - \nu\bar{\epsilon}_\theta \tag{1e}$$

$$\bar{k}_\xi = \bar{M}_\xi/\bar{D} - \bar{k}_\theta\nu \tag{1f}$$

$$\bar{N}_\theta = (\bar{\epsilon}_\theta + \nu\bar{\epsilon}_\xi)/\bar{C} \tag{1g}$$

$$\bar{M}_\theta = \bar{D}(\bar{k}_\theta + \nu\bar{k}_\xi) \tag{1h}$$

$$\bar{\alpha} = \bar{L} + \bar{\epsilon}_\xi \tag{1i}$$

$$\bar{r} = \bar{L}\bar{r}_o + \bar{u} \tag{1j}$$

$$\frac{d\bar{w}}{d\bar{\xi}} = \bar{\alpha}\sin\phi - \bar{L}\sin\phi_o \tag{1k}$$

$$\frac{d\bar{u}}{d\bar{\xi}} = \bar{\alpha}\cos\phi - \bar{L}\cos\phi_0 \tag{1l}$$

$$\frac{d\bar{\beta}}{d\bar{\xi}} = \bar{k}_\xi \tag{1m}$$

$$\frac{d\bar{V}}{d\bar{\xi}} = -\bar{\alpha}\cos\phi(\bar{V}/\bar{r} - \bar{P}\bar{T}) \tag{1n}$$

$$\frac{d\bar{H}}{d\bar{\xi}} = -\bar{\alpha}\{(\bar{H}\cos\phi - \bar{N}_\theta)/\bar{r} + \bar{P}\bar{T}\sin\phi\} \tag{1o}$$

$$\frac{d\bar{M}}{d\bar{\xi}} = \bar{\alpha}\cos\phi(\bar{M}_\theta - \bar{M}_\xi)/\bar{r} - \bar{\alpha}\bar{P}\bar{T}^2 \times (\bar{H}\sin\phi - \bar{V}\cos\phi) \tag{1p}$$

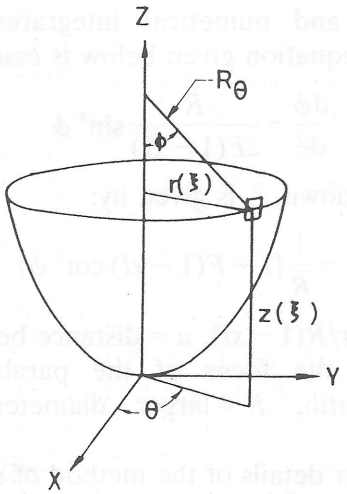

Fig. 1. Middle surface of shell.

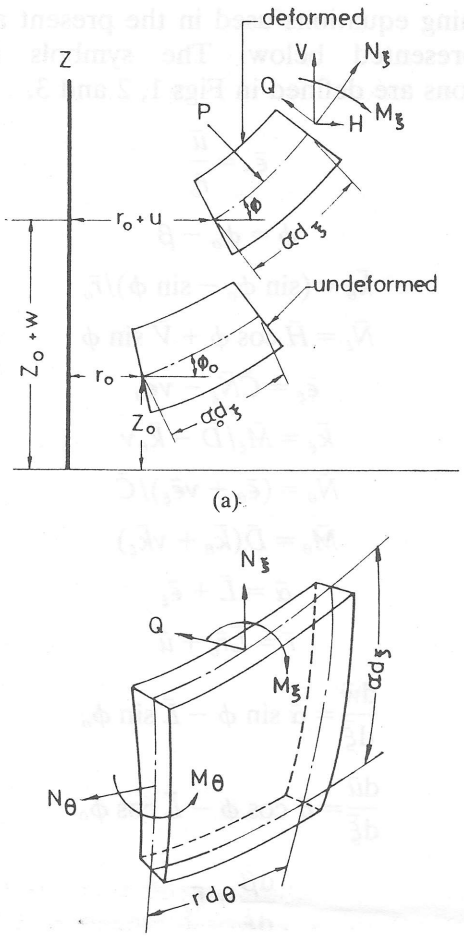

Fig. 2. (a) Side view of element of shell in deformed and undeformed states; (b) element of shell showing stress resultants and couples.

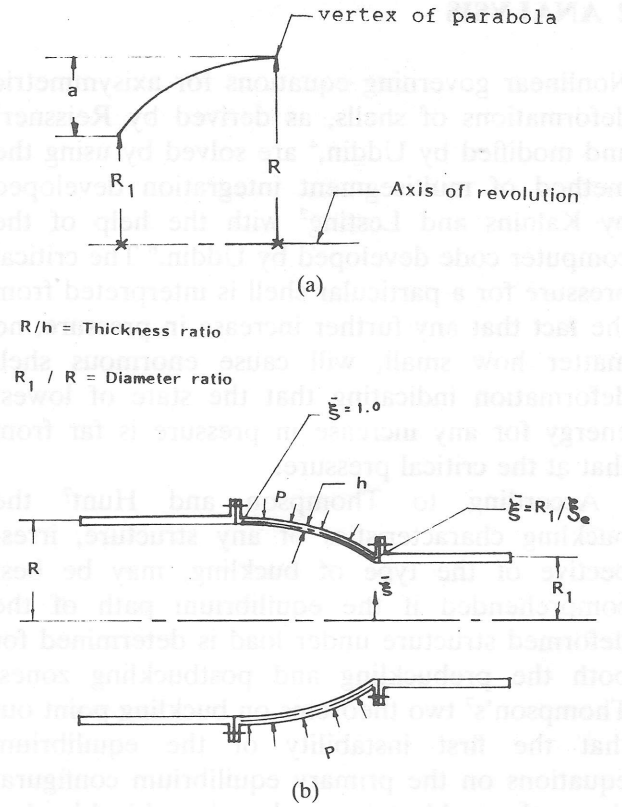

Fig. 3. (a) Geometry of the parabolic reducer; (b) parabolic reducer.

It should be mentioned here that all the normalized parameters in eqns (1) are expressed in terms of the independent variable $\bar{\xi}$. For the case of a parabolic reducer there is no closed form expression for the normalized parameters ϕ_o and $\bar{r}_o$ and numerical integration of the differential equation given below is essential.

$$\frac{d\phi}{d\bar{\xi}} = \frac{\bar{R}}{2F(1-xl)} \sin^3 \phi \qquad (1q)$$

Once ϕ is known, $\bar{r}_o$ is given by:

$$\bar{r}_o = \frac{1}{\bar{R}} \{1 - F(1-xl) \cot^2 \phi\} \qquad (1r)$$

where, $F = a/R(1-xl)$, a = distance between the vertex and the focus of the parabola, xl = diameter ratio, R = larger diameter of the reducer.

For further details of the method of solution of the six differential eqns (1k) to (1p) along with the boundary conditions in eqns (2) and (3), interested readers may refer to Ref. 4.

3 BOUNDARY CONDITIONS

For the general case of axisymmetric deformations of shells of revolution it was shown by Uddin[4] that the boundary conditions at the edges require the specification of $\bar{H}$ or $\bar{u}$, $\bar{M}_\xi$ or $\bar{\beta}$, and $\bar{V}$ or $\bar{w}$. In the present analysis, considering both the larger and the smaller diameters of the reducer sufficiently large and flange connected, it is quite justified to assume that both the ends are fixed or clamped. This will also help us to compare the results with Ref. 1 where exactly the same boundary conditions were used. Hence, the condition at the larger end of the reducer is specified as:

$$\bar{u} = 0, \quad \bar{\beta} = 0, \quad \bar{w} = 0 \qquad (2)$$

and at the smaller end:

$$\bar{u} = 0, \quad \bar{\beta} = 0, \quad \bar{w} = 0 \qquad (3)$$

4 SOLUTION

The same method of multisegment integration as used by Uddin[4] for nonlinear analysis of pressure vessels has been employed here with boundary conditions given in eqns (2) and (3). To determine the buckling pressure the program starts with an assumed load $\bar{P}$ and an incremental load step $\Delta\bar{P}$, and then solves the nonlinear governing equation at each load step with a pre-assigned convergence criteria. If the solution fails to converge at any load step, the load step $\Delta\bar{P}$ is automatically halved and the solution is again attempted. The critical pressure is anticipated from the load/displacement curves as the branching point or limit point of the two distinct modes of deformation. Consequently, it is always the bifurcation point where the solution fails to converge.

5 RESULTS AND DISCUSSION

The summary of the results of the analysis referring to variation of diameter ratio and thickness ratio is presented in Figs 4 and 5.

Table 1 gives a comparison of critical pressures between a parabolic and a conical reducer with identical parameters. It should be mentioned here that the same boundary conditions, that is clamped edges, are assumed for the comparison. It is seen that the critical load is always higher for a parabolic reducer. For a diameter ratio of 0·5 and thickness ratio of 500, the critical load for a parabolic reducer is 1·8 times greater than that of a conical reducer with an apex angle of 60°, 2 times for an apex angle of 90° and 3·5 times for an apex angle of 120°. The superiority of the stability of the parabolic reducer increases with decreasing thickness and decreasing diameter ratios as can be seen from Table 1. For $R_1/R = 0{\cdot}3$ and $R/h = 1500$, the critical load for a parabolic reducer is 2·2 times greater than that for an identical conical reducer of an apex angle of 60°, 3·3 times greater for an apex angle of 90° and 6 times greater for an apex angle of 120°. It was shown in Ref. 1 that the critical pressure for a conical reducer decreases almost linearly when the apex angle is increased. The highest critical load is thus for the minimum apex angle which was 60° in Ref. 1. It is seen in Table 1 that the critical pressure for a parabolic reducer is almost double the critical pressure for the conical reducer with an apex angle of 60° for the same diameter ratio and thickness ratio.

Figures 4 and 5 show the effect of thickness ratio (R/h) and diameter ratio (R_1/R) on the critical load respectively. Figure 4 provides evidence of the common truth that the thinner the structure, the lower is the critical load. Figure 5 shows that the higher the diameter ratio, the higher is the critical load. Figure 5 also shows that the critical load increases slowly up to a diameter ratio of 0·8 but increases at a faster rate if the diameter ratio is further increased. Of course the effect of the diameter ratio on the

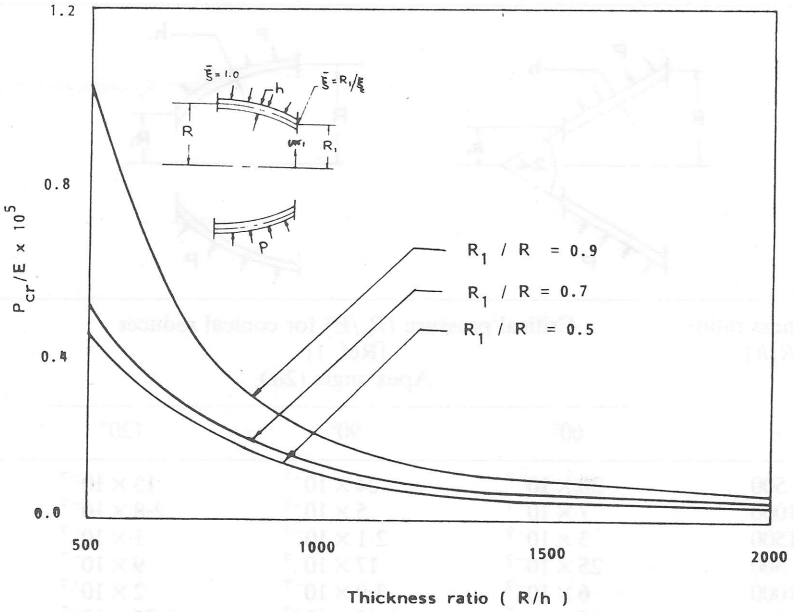

Fig. 4. Critical load versus thickness ratio for a parabolic reducer.

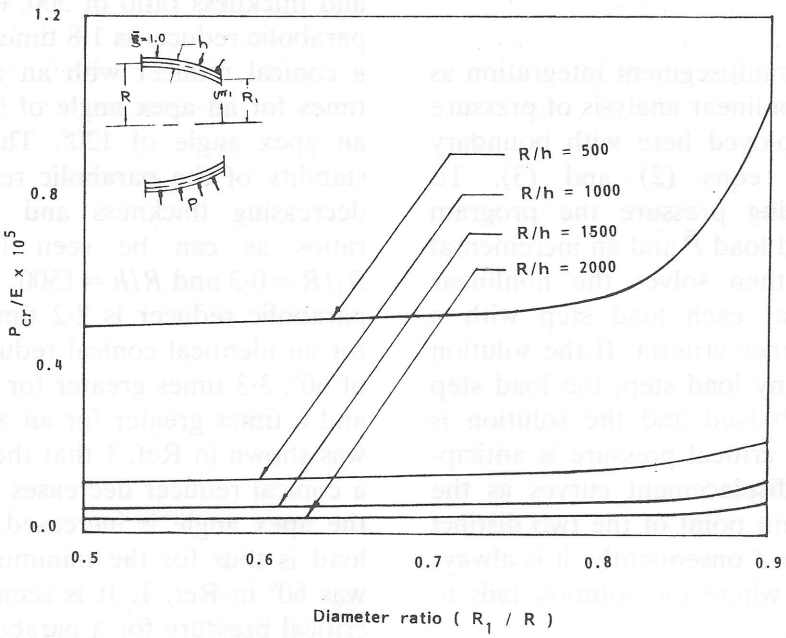

Fig. 5. Critical load versus diameter ratio for a parabolic reducer.

critical load diminishes as the structures are made thinner.

An interesting observation from the present analysis is that the parabolic reducers with higher diameter ratio fail near the smaller end but those with lower diameter ratios fail near the larger end. For ready reference the failure patterns of a reducer with higher diameter ratio (R_1/R) of 0·9 and with a lower diameter ratio of 0·5 are presented in Figs 6(c) and 7(c) respectively. It should be mentioned here that in Figs 6(c) and 7(c), the y-axis corresponds to the nondimentional radial distance (r/R) of the material points on the shell meridian measured from the axis of

Table 1. Comparison of critical pressure between a parabolic reducer and a conical reducer with clamped ends

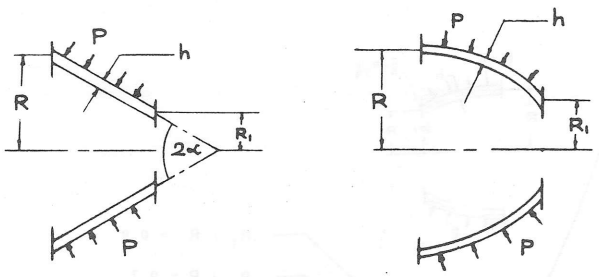

Diameter ratio (R_1/R)	Thickness ratio (R/h)	Critical pressure (P_{cr}/E) for conical reducer [Ref. 1] Apex angle (2α)			Critical pressure (P_{cr}/E) for parabolic reducer [present analysis]
		60°	90°	120°	
0·5	500	30×10^{-7}	24×10^{-7}	13×10^{-7}	51×10^{-7}
	1000	7×10^{-7}	5×10^{-7}	$2{\cdot}8 \times 10^{-7}$	$11{\cdot}4 \times 10^{-7}$
	1500	3×10^{-7}	$2{\cdot}1 \times 10^{-7}$	1×10^{-7}	$5{\cdot}3 \times 10^{-7}$
0·3	500	25×10^{-7}	17×10^{-7}	9×10^{-7}	50×10^{-7}
	1000	6×10^{-7}	$3{\cdot}9 \times 10^{-7}$	2×10^{-7}	$11{\cdot}3 \times 10^{-7}$
	1500	$2{\cdot}65 \times 10^{-7}$	$1{\cdot}60 \times 10^{-7}$	$0{\cdot}85 \times 10^{-7}$	$5{\cdot}02 \times 10^{-7}$

the parabolic reducer. The exaggerated buckled configurations of the reducers are found by calculating the radial and axial displacements of the material points on the shell meridian at loads higher than the critical ones.

In many cases, the structures may pass through a further stable equilibrium position just after the bifurcation point is exceeded; an example is that of snapthrough-type buckling. Our analysis deals with the type of buckling as seen from the load-displacement curves in Figs 6(a) and 6(b), 7(a) and 7(b), where the solution converges after the bifurcation point is exceeded, because the structures pass to a superior stable equilibrium

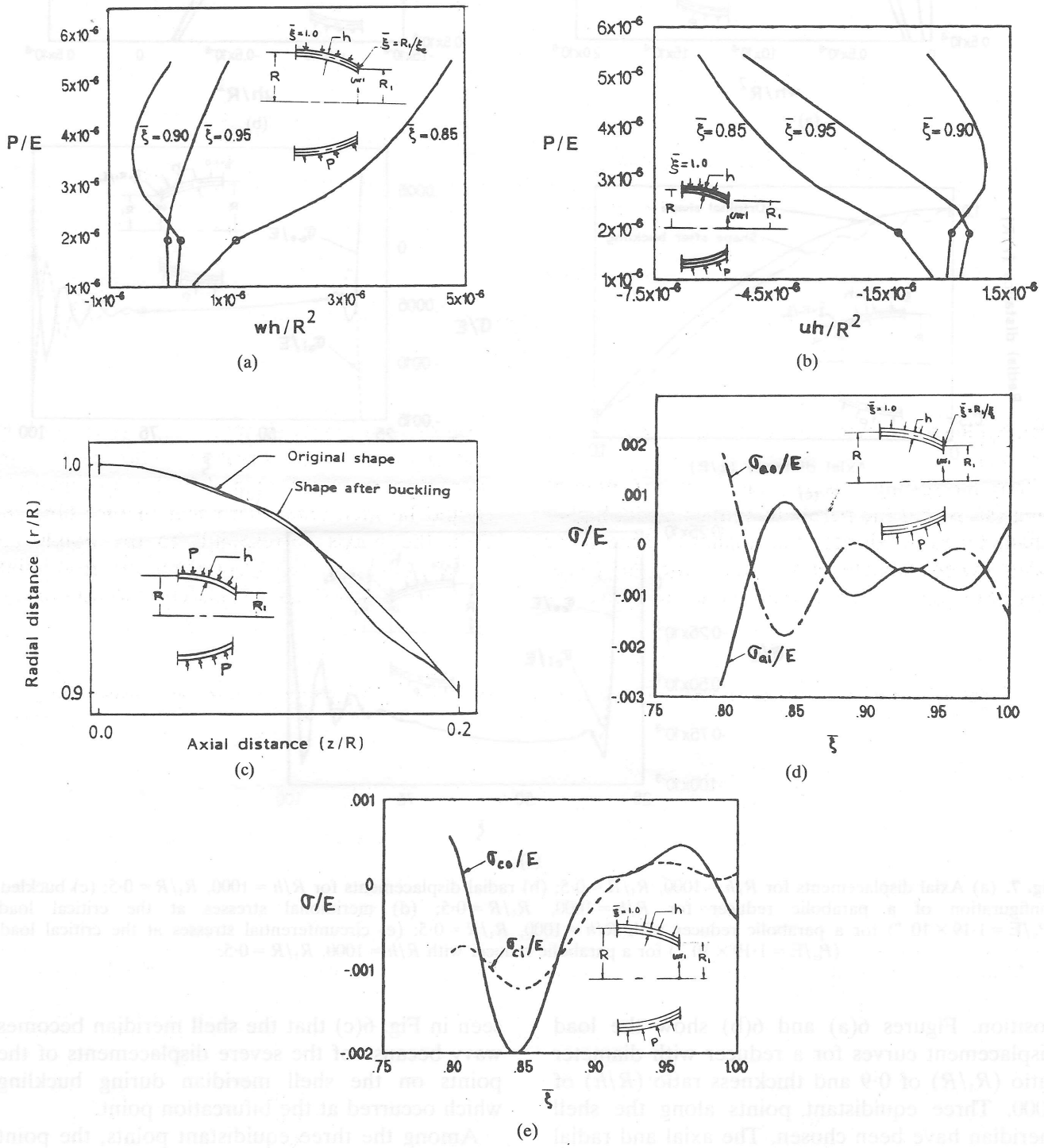

Fig. 6. (a) Load versus axial displacement curve for $R/h = 1000$, $R_1/R = 0{\cdot}9$; (b) load versus radial displacement curve for $R/h = 1000$, $R_1/R = 0{\cdot}9$; (c) buckled configuration of a parabolic reducer for $R/h = 1000$, $R_1/R = 0{\cdot}9$; (d) meridional stresses at the critical load ($P_{cr}/E = 1{\cdot}95 \times 10^{-6}$) for a parabolic reducer with $R/h = 1000$, $R_1/R = 0{\cdot}9$; (e) circumferential stresses at the critical load ($P_{cr}/E = 1{\cdot}95 \times 10^{-6}$) for a parabolic reducer with $R/h = 1000$, $R_1/R = 0{\cdot}9$.

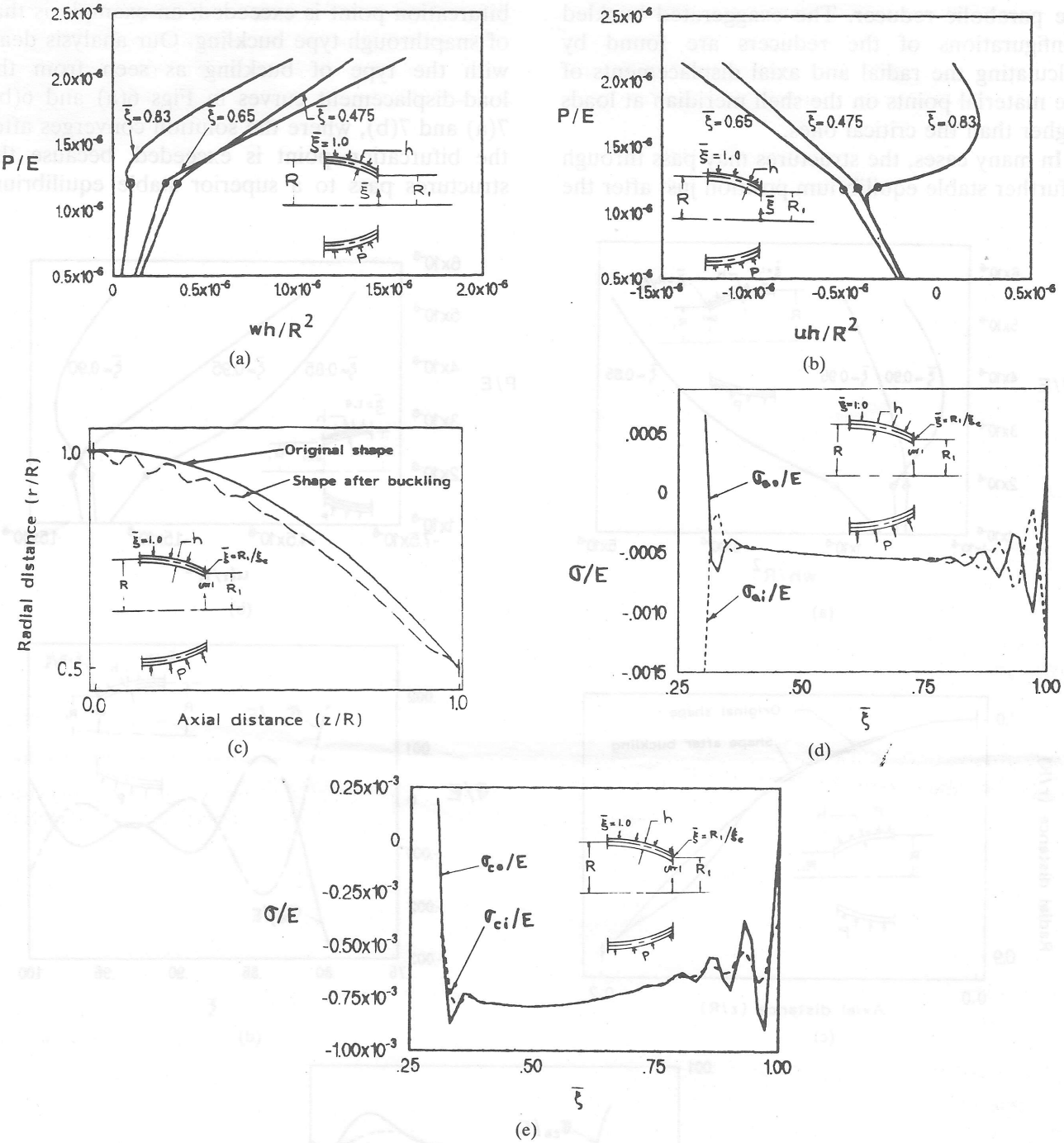

Fig. 7. (a) Axial displacements for $R/h = 1000$, $R_1/R = 0{\cdot}5$; (b) radial displacements for $R/h = 1000$, $R_1/R = 0{\cdot}5$; (c) buckled configuration of a parabolic reducer for $R/h = 1000$, $R_1/R = 0{\cdot}5$; (d) meridional stresses at the critical load ($P_{cr}/E = 1{\cdot}19 \times 10^{-6}$) for a parabolic reducer with $R/h = 1000$, $R_1/R = 0{\cdot}5$; (e) circumferential stresses at the critical load ($P_{cr}/E = 1{\cdot}19 \times 10^{-6}$) for a parabolic reducer with $R/h = 1000$, $R_1/R = 0{\cdot}5$.

position. Figures 6(a) and 6(b) show the load displacement curves for a reducer with diameter ratio (R_1/R) of 0·9 and thickness ratio (R/h) of 1000. Three equidistant points along the shell meridian have been chosen. The axial and radial displacement curves for those three points show clearly how the rate of deformation changes sharply just after the bifurcation point. It is also seen in Fig. 6(c) that the shell meridian becomes wavy because of the severe displacements of the points on the shell meridian during buckling which occurred at the bifurcation point.

Among the three equidistant points, the point at $\bar{\xi} = 0{\cdot}85$, which is in fact at a distance of 25% from the smaller end, is most severely displaced both axially and radially during buckling as can

be seen from the load/displacement curves in Figs 6(a) and 6(b). This results in the initiation of buckling near the smaller end, as can be seen from the buckled reducer presented in Fig. 6(c).

The stresses just prior to buckling are presented in Figs 6(d) and 6(e). The stress curves plotted along the shell meridian are in complete harmony with the failure pattern of a reducer with large diameter ratio. The points at a distance of 25% of reducer length from the smaller end, which are most severely displaced as can be seen from Figs 6(a) and 6(b), are under high meridional and circumferential stresses as seen from Figs 6(d) and 6(e). This combined effect of the two types of stresses causes boundless displacements of the points near $\bar{\xi} = 0{\cdot}85$ and buckling initiates near the smaller end. Among the nondimensional stresses (σ/E) the meridional stress is of the highest magnitude $(-0{\cdot}0028)$ which occurs at the smaller end of the reducer.

Reducers with smaller diameter ratio fail near the base or the larger end, as observed from another set of representative curves for a diameter ratio of 0·5 and thickness ratio of 1000 presented in Figs 7(a) to 7(c). The load displacement curves for three equidistant points along the shell meridian of the reducer are presented in Figs 7(a) and 7(b). The bifurcation point is traced at the junction of two distinct modes of deformation. Among the three equidistant points, the point at a distance of 25% of reducer length from the larger end at $\bar{\xi} = 0{\cdot}83$ is most severely displaced both radially and axially, indicating that buckling initiates near the larger end. Figure 7(c) shows the buckled state of the same reducer. The nondimensional stresses (σ/E) along the shell meridian are presented in Figs 7(d) and 7(e). The sharp perturbation in the stresses near the larger end (around $\bar{\xi} = 0{\cdot}8$ to 1·0) causes the adjacent points on the shell meridian to be displaced randomly in the opposite directions, resulting in crooked deformation of the shell meridian near the base. For this particular reducer the maximum nondimensional stress is the meridional stress in the inner fibre which occurs at the smaller end of the reducer. Its magnitude is $-0{\cdot}00104$ as seen in Fig. 7(d).

Since the nondimensional yield strength (σ_y/E) for this steel is within the range 0·001 to 0·01, so our analysis indicates that the material is within elastic limit. It is found in the present analysis that the meridional stress is higher than the circumferential stress. Hence, meridional or symmetric buckling is likely in this type of reducer.

6 CONCLUSION

The present analysis shows that, for values of parameters, a parabolic reducer is superior to a conical reducer regarding stability and that this superiority increases with increasing thinness and decreasing diameter ratio.

It has also been observed that for a parabolic reducer, the diameter ratio influences the critical load but its effect diminishes for thinner reducers. The present analysis is based on large deflection analysis of the shells and does not include approximations which would force the shell element to buckle in a predetermined manner. It is therefore considered that the results obtained are likely to be very accurate.

REFERENCES

1. Ali, G. M. Zulfikar, Stability and stress analysis of conical reducers, MSc Engineering thesis, Bangladesh University of Engineering and Technology, Dhaka (1991).
2. Kalnins, A. & Lestingi, J. E., On nonlinear analysis of elastic shells of revolution. *J. Appl. Mech., Trans. ASME* **34** (1967) 59.
3. Reissner, E., *On the Theory of Thin Elastic Shells.* H. Reissner Anniversary Volume, J. W. Edwards, Ann Arbor, Michigan (1949) 231.
4. Uddin, Md. W., Large deflection analysis of composite shells of revolution, PhD thesis, Carleton University, Canada (1969).
5. Uddin, Md. W., Buckling of general spherical shells under external pressure, *Int. J. Mech. Sci.,* **29** (7) (1987) 469–481.
6. Uddin, Md. W., A computer program for nonlinear analysis of pressure vessels, *Int. J. Press. Ves. & Piping,* **22** (1986) 271–309.
7. Thompson, J. M. T. & Hunt, G. W., *A General Theory of Elastic Stability,* John Wiley and Sons, London, U.K. (1973).
8. Dumir, P. C. & Khatri, K. N., Axisymmetric static and dynamic buckling of orthotropic shallow conical caps, *AIAA Journal,* **23** (1985) 1762–1767.
9. Dumir, P. C. & Khatri, K. N., Axisymmetric static and dynamic buckling of orthrotropic truncated shallow conical caps, *Comp. & Struct.,* **22** (1986) 335–342.
10. Thurston, G. A., A numerical solution of the nonlinear equations for axisymmetric bending of shallow spherical shells, *Journal of Applied Mechanics, Trans. ASME,* **28** (1961) 557.
11. Archer, R. R., Stability limits for a clamped spherical

shell segment under uniform pressure, *Q. Appl. Math.* **15** (1958) 355.
12. Huang, N. C., Axisymmetric dynamic snap-through of elastic clamped shallow spherical shells, *AIAA Journal,* **7** (1969) 215.
13. Huang, N. C., Unsymmetrical buckling of thin shallow spherical shells, *J. Appl. Mech., Trans. ASME,* **31** (1964) 447.
14. Ganapathi, M. & Varadan, T. K., Dynamic buckling of othrotropic shallow spherical shells, *Comp. & Struct.,* **15** (1982) 517.
15. Nath, Y., Dumir, P. C. & Gandhi, M. L., Choice of collocation points for axisymmetric nonlinear two-point boundary value problems in static or shallow spherical shells, *Engng. Trans.,* **31,** (1983) 331.
16. Dumir, P. C., Gandhi, M. L. & Nath, Y., Axisymmetric static and dynamic buckling of orthrotropic shallow spherical caps with flexible supports, *Acta Mech.* **52** (1984) 93.
17. Bushnell, D., BOSOR5 program for buckling of elastic–plastic complex shells of revolution including large deflection and creep, *Comput. Struct.* **6** (1976) 221.
18. Bushnell, D., BOSOR4 program for stress, buckling and vibration of complex shells of revolution, *Structural Mechanics Software Series* (Edited by N. Perrone and W. Pilkey), University Press of Virginia (1977), 11–143.
19. Mondkar, D. P. and Pawell, G. H., ANSR, a general-purpose computer program for analysis of nonlinear structural response, *4th SMiRT Conf., Paper M1/4*, San Francisco (1977).
20. Almroth, B. O., Brogan, F. A. & Stanley, G. M., Structural analysis of general shells, Vol. 11: User Instruction for STAGSC. Lockheed Missiles & Space Co., Report LMSC–D633873 (1979).
21. Bushnell, D., Nonsymmetric buckling of internally pressurized ellipsoidal and torispherical elastic–plastic pressure vessel heads, *J. Press. Vessel Technol,* **99** (1977) 54.
22. Bushnell, D., Elastic–plastic buckling of internally pressurized torispherical vessel heads, *Nuclear Engng Des.,* **48** (1978) 405.
23. Bushnell, D. and Galletly, G. D., Stress and buckling of internally pressurized elastic–plastic torispherical vessel heads, comparison of tests and theory, *J. Press. Vessel Technol.* **99** (1977) 39.
24. Bushnell, D., Elastic–plastic buckling of internally-pressurized ellipsoidal pressure vessel heads, *Welding Research Council Bulletin 267*, United Engineering Centre, New York (1981).
25. Bushnell, D., Plastic buckling of various shells, *J. Press. Vessel Technol.,* **104** (1982) 51.